Cryo-XPS for Surface Characterisation of Nanomedicines

David J. H. Cant 0000-0002-4247-5739,[1] Yiwen Pei 0000-0001-6976-5560,[1] Andrey Shchukarev 0000-0002-4766-2672,[2] Madeleine Ramstedt 0000- 0003- 2646- 8501,[2] Sara S. Marques 0000-0002-4386-850X,[3] Marcela A. Segundo 0000-0003-2938-0214 ,[3] Jeremie Parot,[4] Alicja Molska,[4] Sven E. Borgos,[4] Alexander G. Shard 0000-0002-8931-5740,[1] Caterina Minelli 0000-0002-8092-251X [1]**

[1]National Physical Laboratory, Hampton Road, Teddington, TW11 0LW, UK

[2]Department of Chemistry, Umeå University, 901 87 Umeå, Sweden

[3]LAQV, REQUIMTE, Department of Chemical Sciences, Faculty of Pharmacy, University of Porto, R. Jorge Viterbo Ferreira 228, 4050-313 Porto, Portugal

[4]Department of Biotechnology and Nanomedicine, SINTEF Industry, 7465 Trondheim, Norway

Keywords: Nanomedicine; Nanoparticle; XPS; Cryo; Surface Chemistry; LNP; PEG

ABSTRACT

Nanoparticles used for medical applications commonly possess coatings or surface functionalities intended to provide specific behaviour *in vivo*, for example the use of PEG to provide stealth

properties. Direct, quantitative measurement of the surface chemistry and composition of such systems in a hydrated environment has thus far not been demonstrated, yet such measurements are of great importance for the development of nanomedicine systems. Here we demonstrate the first use of Cryo-XPS for the measurement of two PEG-functionalised nanomedicines: a polymeric drug delivery system and a lipid nanoparticle mRNA carrier. The observed differences between Cryo-XPS and standard XPS measurements indicate the potential of Cryo-XPS for providing quantitative measurements of such nanoparticle systems in hydrated conditions.

INTRODUCTION

Nanoparticles are used as drug delivery vehicles to protect the therapeutic cargo and improve the intracellular delivery, and therefore bioavailability and potency, of small and large molecules[1–5]. Particles in the blood stream in the size range between 60 nm and 400 nm[6] are found to accumulate at the tumour site due to the defective vasculature architecture of tumour vessels, which prompted a significant interest in the use of nanoparticles for cancer treatment applications[3]. The recent pandemic has brought onto centre stage the use of lipid nanoparticles (LNP) for the protection and delivery of oligonucleotides for vaccine applications[7]. For nanoparticles to be used in the body, certain features are critical – the complex nanomedicine, comprising both the active ingredient and the delivery vehicle, must have favourable therapeutic index, be effective at reaching the desired target, and present a favourable pharmacokinetic profile for an effective dose to be applied.

It is well known that particle surface chemistry affects how nanomaterials interact with the biological environment. In order to maximise the circulation time of nanomedicines within the body, a common strategy consists of functionalising the external surface of the nanoparticles with poly(ethyleneglycol) (PEG, also known as polyethylene oxide) moieties. PEG is known for

providing 'stealth' properties – allowing the particle to avoid clearance mechanisms thus increasing time spent in circulation,[8,9] and potentially providing other benefits depending on the specific system, including improved stability and reduced immunogenicity.[10–12]

For therapeutic nanomaterials PEGylation is widespread, with the majority of nanomedicines currently in use incorporating PEG.[13] For polymer-based nanomedicines, for example, surface coverage of the PEG layer can have more profound effects than nanoparticle size in determining clearance rate in-vivo[14]. In the case of LNPs, the presence of PEG on the surface is integral to the mechanism of particle formation. It is thought in fact that particles produced by the rapid mixing microfluidic approach are initially stabilised by attractive electrostatic interactions between the cationic lipids and anionic nucleic acids present. The particles fuse together and grow in size as the pH of the solution is raised to neutral and the lipids lose their charge, until the density of the PEG layer at the surface of the particles is such to impart steric stabilisation[15]. The ability to interrogate the external PEG layer is of great advantage to gain further understanding and control of product development and performance. However, key characteristics such as the chemical composition, chain orientation and distribution, layer thickness and density of this PEG coating are rarely identified, with characterisation typically focussing on indirect measurements including liquid chromatography, liquid-based particle size methods, and infrared or Raman-based spectroscopies.[13] While transmission electron microscopy (TEM) is sometimes used for structural characterisation, this may have drawbacks in terms of the limited statistical representation of the sample, instability of soft matter samples under the electron beam, the low contrast for purely organic nanomaterials, and the difficulty of their chemical identification, which make quantitative measurements challenging. In addition, cryogenic preparation is often required to image these materials to achieve a close-to-native environment, i.e. representative of the hydrated conditions.

High vacuum chemical analysis tools such as X-ray photoelectron spectroscopy (XPS), time-of-flight secondary ion mass spectrometry (TOF-SIMS) and atomic probe tomography have been successfully used to localise, identify and quantify the chemical composition of nanoparticles and their coatings. Their broad application to nanomedicine systems holds significant potential in answering some critical question around, for example, the successful encapsulation of the therapeutically active molecules, their degradation or release mechanism. The same methods would also allow the measurement of particle coatings that are rationally engineered to increase circulation times and enable active targeting of disease sites. However, introducing soft matter particles in the vacuum environment while preserving their structure is a significant technological challenge and a number of strategies have been developed to overcome this obstacle[16]. One of the most common methods for analysis of vacuum-sensitive materials is the use of near-ambient-pressure (NAP) techniques such as NAP-XPS. This may be achieved in a number of ways, most of which involve holding the sample at a given pressure with differential pumping providing a sharp gradient towards UHV conditions closer to the detector. This typically requires instrumentation designed specifically for this purpose and may necessitate care in calibration to account for the NAP environment. Similarly to TEM, cryogenic preparation of such samples has also been employed with some success[17–19]. Cryogenic sample handling relies on a sample fast-freezing technique where amorphous water is maintained at the solid sample surface by rapidly freezing a hydrated sample. Thus, it is believed that the frozen sample prepared using this technique is structurally representative of the hydrated materials. Cryogenic preparation and vacuum analysis, such as XPS and TOF-SIMS, have been successfully utilised for measuring surface chemical compositions of a range of soft-matter samples, including polymer films[20,21] and hydrogels [22], lipid bilayers [23] and microorganisms (e.g., fungi, bacteria and viruses).[24] While

cryogenic vacuum analysis has been employed to investigate the hydrated layers on flat surfaces, there is lack of understanding in the chemistry of nanoparticle coatings in cryo-hydrated state.

XPS is a highly surface sensitive, quantitative chemical analysis technique which has demonstrated efficacy in providing both compositional and structural information on nanoparticulate samples.[25–30] Unlike conventional XPS, cryo-XPS enables measurement of the samples in a near-to-native state, therefore avoiding alteration to their structure due to the lack of stability in vacuum or during processes such as lyophilisation, or to the chemistry due to the introduction of preservatives.[31] Cryo-XPS may therefore represent an avenue to obtain quantitative structural and chemical information on the coatings and surfaces of nanoparticles for medical applications.

Here we apply for the first time cryo-XPS to analyse organic nanoparticles in a vitrified state, thus retaining a hydrated environment. Two nanoparticle systems are investigated: a poly-lactide-*co*-glycolide (PEG-PLGA) drug carrier; and an LNP system for mRNA delivery. Polymeric and lipidic nanoparticles are among the most produced for drug delivery aims[32–36], with lipid NPs being the most approved for clinical use[37]. We focus the work on the analysis of the particle coatings and show the potential of this method for the retention of the expected nanoparticle structure in suspension.

METHODS

POLYMERIC NANOPARTICLE PREPARATION AND CHARACTERISATION

Poly(ethylene) glycol methyl ether-block-poly-D,L-lactide-co-glycolide (PEG-PLGA) nanoparticles were prepared following the single emulsion-solvent evaporation technique described elsewhere with slight modifications [38]. Briefly, 40 mg of PEG-PLGA polymer (acquired

from Sigma Aldrich, St. Louis, MO, USA, containing PEG with a mean molecular weight (MW) of 2,000, and PLGA with a 50:50 lactide:glycolide ratio and a mean MW of 11,500) were dissolved in 3 mL of acetone (VWR Chemicals, Radnor, PA, USA). After polymer dissolution, this organic phase was slowly added to 5 mL of a 1 % (w/v) polyvinyl alcohol aqueous solution (MW 13,000 – 23,000, 87-89 % hydrolysed), and submitted to probe sonication (VCX130, Sonics and Materials, 115 Newtown, CT, USA) for 1 min, at 70 % amplitude. At the end of the treatment, 15 mL of a 0.1 % (w/v) PVA solution were then added to the resultant. The final emulsion was stirred overnight in open reservoirs at room temperature for acetone removal.

Clofazimine-loaded PEG-PLGA nanoparticles were prepared likewise by dissolution of the 40 mg of PEG-PLGA in 3 mL of solution containing 1.25 mg mL^{-1} of clofazimine (Sigma-Aldrich) prepared in acetone.

The obtained nanoparticles were characterized regarding their particle size and polydispersity by dynamic light scattering (ZetaPALS Analyzer, Brookhaven Instrument Corps, Holtsville, NY,USA). Measurements were performed at 20 °C, using a light incidence angle of 90°, a wavelength of 660 nm, and a refractive index of 1.59. The fresh colloidal dispersions were diluted in ultrapure water (filtered once at 0.22 μm) up to a suitable concentration, and analysed in multiples runs ($n = 6$)

Both placebo and loaded nanoparticles were submitted three times to a washing procedure in ultrapure water by centrifugation (18 000 ×*g*, 25 min, at 20 °C), to remove elements present in the media that did not form particles (*e.g.* PVA, acetone, and free clofazimine in the case of loaded nanoparticles). After this washing procedure, the nanoparticles were freshly analysed by dynamic light scattering regarding their size and polydispersity. The purified nanoparticles and the supernatants from the washing procedure were analysed by HPLC (Jasco system, Jasco, Easton,

USA) for encapsulation efficiency and drug loading determinations. The washed particles were subsequently submitted to further purification by ultrafiltration, using Amicon® ultrafiltration devices (Merck Millipore, Darmstadt, Germany) of regenerated cellulose with a 50 kDa filter pore. For this, the washed particles were diluted 38 times in ultrapure water, inserted on the Amicon devices and centrifuged for 15 min, at 2100 ×*g* and at room temperature. Chemical structures of the components of the polymeric nanoparticles are provided in Figure S1 in the supporting information.

LIPID NANOPARTICLE (LNP) FORMULATION AND CHARACTERISATION

LNP formulations were prepared using the following protocol: Briefly, the ionizable cationic lipid D-Lin-MC3-DMA (MedChemExpress), the helper lipid distearoyl-sn-glycero-phosphocholine, (18:0 PC, or DSPC, Avanti Polar Lipids), cholesterol (Sigma-Aldrich, Cat# C8667), the PEG lipid dimyristoyl-rac-glycero-methoxypolyethylene glycol (DMG-PEG2000, Avanti Polar Lipids) were dissolved in pure ethanol with a molar ratio of 50:10:38.5:1.5 and a total lipid concentration of 10 mM. Firefly luciferase (FLuc) mRNA from Trilink (TriLink BioTechnologies) was diluted in acetate buffer 25 mM (pH 4). The molar ratio of the amine groups on the ionizable lipid to the phosphate groups on mRNA (i.e., the N/P ratio) was kept at 5.

The LNP was formulated using a T-junction (IDEX Health and Science) coupled by two syringe pumps (New Era Pump Systems). The lipid ethanol solution and the mRNA aqueous solution were injected into the T junction at a flow rate of 1 mL min^{-1} and 3 mL min^{-1}, respectively. The collected LNP suspension was dialyzed against 1000-fold volume of phosphate-buffered saline (PBS) at pH 7.4 (to remove ethanol and raise the pH to physiological pH) for 12 h with a molecular weight cut-off (MWCO) of 10 kDa (Slide-A-Lyzer™ Dialysis Cassettes, ThermoFisher). The LNPs were

characterized immediately following dialysis for hydrodynamic radius and polydispersity index using a dynamic light scattering VASCO KIN (Cordouan Technologies, Pessac, France), mRNA concentration and lipid concentration using HPLC-mass spectrometry.

Chemical structures of the components of the lipid nanoparticles are provided in Figure S2 in the supporting information. The RNA payload typically forms assemblies with the ionizable lipids via electrostatic interactions that are surrounded by stabilizing lipids such as cholesterol. The PEGylated lipids are expected to form an outer layer at the surface of the particle.

CRYO-XPS INSTRUMENTATION

XPS spectra were recorded using an Axis Ultra DLD electron spectrometer (Kratos Analytical Ltd., UK). A monochromated Al Kα x-ray source was used, operating at a beam current of 10 mA and voltage of 15 kV. Measurements were acquired in hybrid mode using a magnetic lens, with an analysis area of 300 μm x 700 μm. Charge neutralization was used for the measurements. Data were processed in Casa XPS version 2.3.22; spectra were corrected for energy-dependent instrumental-transmission using the NPL transmission function correction[39], and the binding energy (BE) scale was referenced to the C 1s line of aliphatic carbon, set at 285.0 eV. Peak areas were quantified through application of a Tougaard background-subtraction and the use of NPL average-matrix relative-sensitivity factors[40]. For cryogenic measurements, a small (approx. < 7 μL) droplet of the sample suspension was fast frozen on a sample holder cooled to <-170 °C in the load-lock of the instrument, which was then immediately sealed and pumped to vacuum. Samples were then transported to the analysis stage, kept at <-150 °C, throughout the measurement. A detailed experimental protocol for the cryo-XPS is published elsewhere[41]. Dry

samples were prepared by drop-casting of the particles in suspension directly onto the sample holder at room temperature.

RESULTS AND DISCUSSION

XPS measurements were performed on both dry nanoparticle deposits (drop cast directly onto the sample holder at ambient temperature for the LNP system, and dried from frozen *in-situ* for the polymeric system), and cryogenically frozen nanoparticle suspensions for both the LNP and polymer systems. Survey spectra were acquired for all the samples (see Figures S3 and S4 in the supporting information) along with high-resolution spectra for core levels of interest. Carbon 1s spectra and associated fits are shown in Figure 1 and Figure 3 for the polymeric and LNP samples respectively. Both Figure 1 and Figure 3 show the results of the XPS measurements performed on the sample prepared in the cryogenic (left panels of figures) as well as the dry (right panels of the figures) states. Homogeneous-equivalent atomic concentrations for each sample, determined from survey spectra are reported in the supporting information, tables S1 to S4. The reported oxygen concentration includes a significant contribution from the water in which the particles are suspended, which cannot be reasonably separated from the oxygen within the particles themselves through peak fitting (Figure S7). While both systems consist of materials that may be sensitive to damage from the x-ray beam and secondary electrons, no significant changes were observed in relative peak intensities between the survey and high-resolution spectra acquisition, so it is likely that any damage occurs on a long enough timescale to be considered negligible.

POLYMERIC NANOPARTICLES

For the polymeric particles, the carbon 1s spectra were fitted with components corresponding to: PLGA (with 50:50 glycolide:lactide ratio); PVA (poly-vinyl alcohol with a small proportion of acetate[42]); a single C-O peak for PEG; and the drug molecule. All peaks within the fit were constrained relative to other peaks from the same material in terms of binding energy, full width at half maximum, and area, based on their chemical structure and literature data[42,43]. The PEG peak was constrained to within reasonable deviation from the expected literature position, and intensity of the components related to the drug molecule were constrained based on the amount of nitrogen measured from the survey.

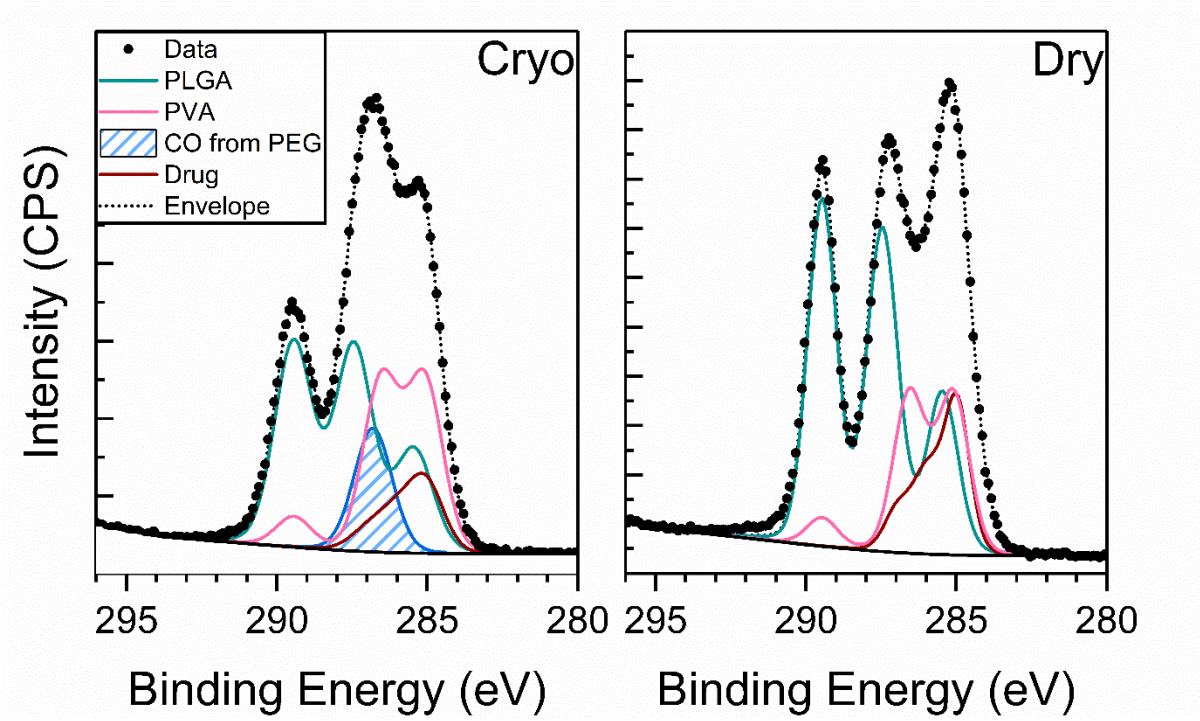

Figure 1- Carbon 1s spectra for the polymeric particles, analysed by both cryo-XPS in a hydrated state, and room-temperature XPS dried onto the sample holder. Peak fits are based on the structure of the pure monomer materials. The drug component is constrained based on chemical structure of the drug, clofazimine, relative to the nitrogen signal from the survey spectra.

Based on the molar mass of the PEG-PLGA copolymer used, we can define three extreme cases for the particle structure and calculate an indicative ratio of PEG to PLGA that would be observed for each. These three cases are: 1) PEG entirely localised at the surface; 2) random orientation, i.e. PEG and PLGA forming an effectively homogeneous mix; and 3) PEG buried beneath the PLGA. It should be noted that PVA was added in the PEG-PLGA nanomedicine formulation as a free-flowing surfactant to provide additional colloidal stability of the PEGylated particles. Therefore, it is expected that PVA remains on the surface in any of the aforementioned cases. Table 1 shows rough indicative ratios of PEG to PLGA signal based on a simple planar model for each case, alongside the observed ratio from the peak fits. Peak fits as a percentage of total carbon 1s signal are given in Table S5. A schematic representation of the models is given in Figure 2, however it should be noted that the true structure must contain a mix of PLGA and PEG within the core due to the size of the particles compared to the polymer chain lengths.

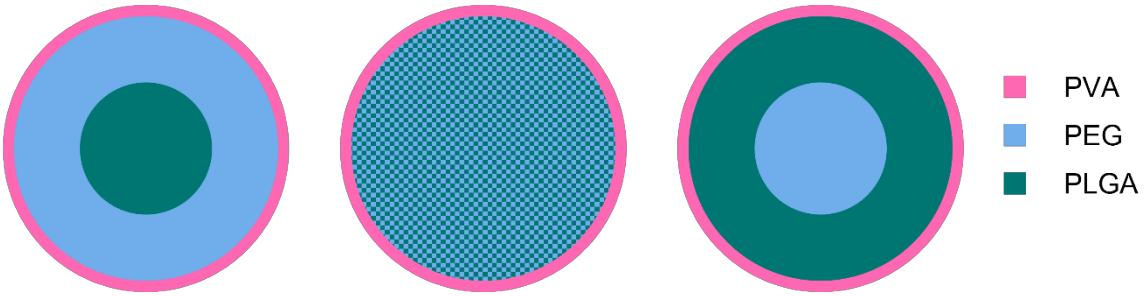

Figure 2 - Schematic of the three considered cases for the polymer particles, from left to right: surface localised PEG; homogeneous mix of PEG/PLGA; buried PEG.

Table 1 - PEG:PLGA equivalent homogeneous ratios for both dry and cryo XPS measurements of polymeric particles, alongside indicative values for the ratios of PEG to PLGA for surface localised PEG, buried PEG, and a homogeneous mix of the copolymer.

Component	Observed Ratio (Dry)	Observed Ratio (Cryo)	Indicative Ratio (Surface PEG)	Indicative Ratio (Homogeneous)	Indicative Ratio (Buried PEG)
PEG:PLGA equivalent homogeneous ratio	No observed PEG signal	0.24	3.0	0.21	0.04

For the dry XPS measurements, as shown in Figure 1, a fully constrained fit to the data with no contribution from the PEG can be obtained, while for the cryo-XPS measurements, a PEG component is required to achieve a reasonable fit. In both cases, the PEG:PLGA ratio is much lower than the indicative value for surface-concentrated PEG. For the cryo-XPS fit the PEG:PLGA ratio lies very slightly above the indicative value for a homogeneous mix. The significant increase in the relative PEG signal for the cryo-XPS compared to the dry XPS measurements indicates a structural difference in which PEG is more surface localised under the hydrated conditions of cryo-XPS. The PEG content in both fits is potentially underestimated due to overestimation of the PVA content. The PVA concentration in the fit is largely determined by the HC component and will be influenced by the presence of unaccounted-for hydrocarbon. If a variable hydrocarbon component is introduced into the fit, unique solutions cannot be found, because the PVA and PEG plus hydrocarbon components are highly correlated.

Environment-induced surface rearrangement of polymer chains is not uncommon[21,22,44,45] . The adopted arrangement of polymer chains on a surface is determined by the affinity between polymer chains and their local environment. Polymer chains tend to rearrange themselves (e.g., expansion, collapsing and sometimes migrating to underlayers) to achieve the lowest surface free energy when transferred between an aqueous, hydrated environment and a dry condition. While the surface rearrangement of polymers on flat surfaces has been studied by several groups,[44,46] the hydrated

surface chemistry and structure of heterogeneous polymer nanoparticles has, to our knowledge, not previously been directly investigated. The differences we observe between the dry and cryo-XPS results indicate that while the drying process likely causes rearrangement of the nanoparticle structure, cryo-XPS measurements allow the hydrated structure to be clarified.

LIPID NANOPARTICLES

Fitting of the carbon 1s spectra for the lipid nanoparticles needs to account for identical chemical environments arising from multiple possible sources. Peaks were assigned as generic carbon moieties – C-C at 285.0 eV, C-O in the range 286.7-287.0 eV, and O=C-O at ~289.0 eV, alongside the characteristic PEG C-O species at 286.4- 286.7 eV, which can arise only from the DMG-PEG within the particle, and the $C\text{-}N^{+}$ species at ~286.2 eV, which arises only from the DSPC component[43]. The peak fits are shown in Figure 3.

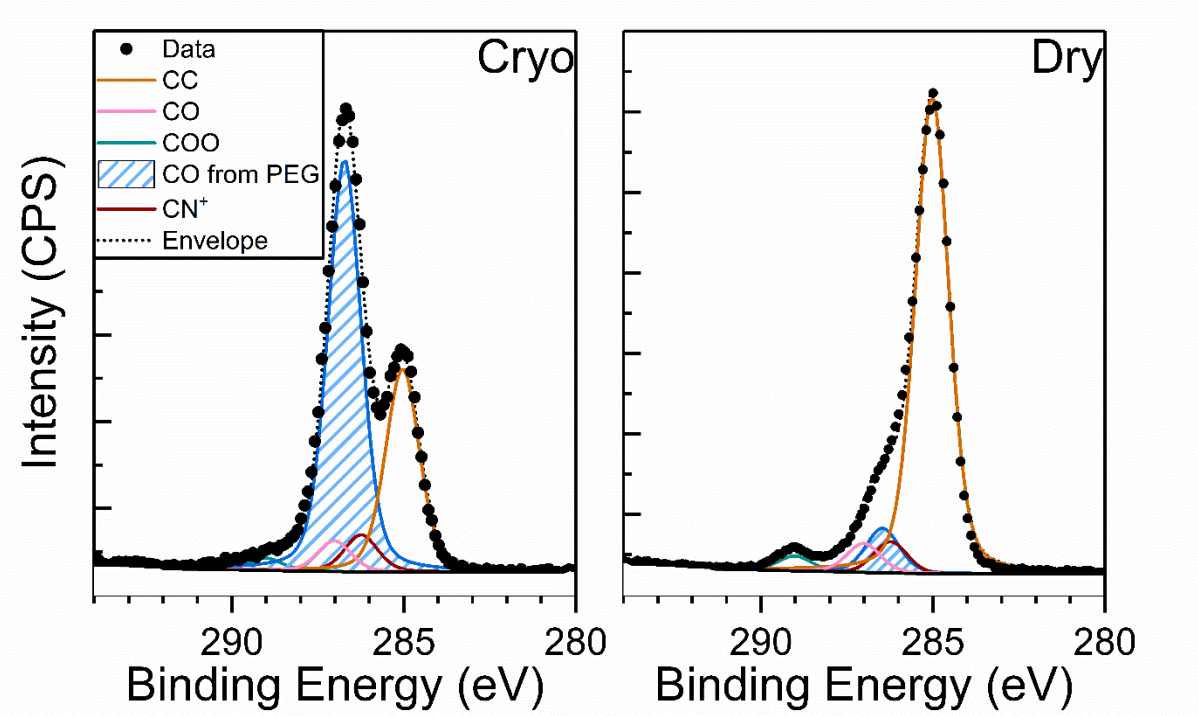

Figure 3 - Carbon 1s spectra for the lipid particles, analysed by both cryo-XPS in a hydrated state, and room-temperature XPS dried onto the sample holder. The CN^+ component is constrained based on nitrogen signal from the survey spectra, to within 10% of the expected intensity.

The molar concentration of PEG within the lipid particles is less than 1.5 %. Therefore the observation of significant intensity attributed to PEG in the cryo-XPS carbon 1s spectrum is notable. This indicates that the PEG is either located at the surface of the particle, or was in solution. From the PEG C-O and DSPC C-N^+ peaks, we can model possible structures for the particle surface, and the intensities of the other peaks corresponding to DSPC and DMG-PEG can be estimated. Two such models are considered: a homogeneous model in which the intensity ratio of the peaks corresponding to each species is equivalent to the chemical formula; and an oriented model, in which the molecules are oriented with the PEG and C-N^+ towards the surface for the DMG-PEG and DSPC respectively. In the oriented model, the contribution to the signal from

components other than the DMG-PEG and DSPC are negligible due to attenuation through these outer layers. When comparing the modelled data to that observed from experiment, the greatest deviation is seen in the concentration of the C-C peak. A comparison of the expected C-C intensity for each model, compared to the observed values, is shown in Figure 2.

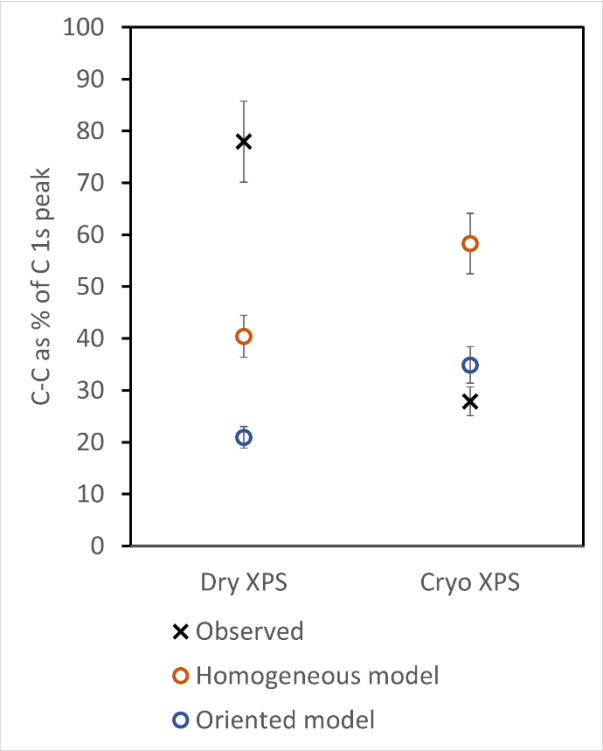

Figure 4 - Intensity of C-C peak as a percentage of the C 1s fit compared to expected values for homogeneous and oriented models. Error bars are based on an estimated 10% uncertainty in peak fitting.

For the cryo-XPS results, when accounting for all the C 1s signal which can reasonably be associated with the DSPC and DMG-PEG, significantly less C-C intensity is observed compared to the expected homogeneous-equivalent composition. There is still a slight deficit in C-C compared even to the oriented model, but this indicates that the cryo-XPS results are considerably closer to the oriented model than the homogeneous model, which would predict an even greater

C-C intensity. Modelled values also assume the PEG is in a 'mushroom' conformation[47] – deviation from this conformation towards an extended 'brush' conformation may cause the slight deficiencies in species, as greater attenuation of the non-PEG signal will occur. The peak intensities as a percentage of the total C 1s signal, alongside the model values, are given in the supporting information.

Due to the size of these molecules, in the oriented case the signal from any material underneath the surface layer will be almost negligible due to electron attenuation through the overlayer. This allows for the relative concentration of the PEG to be interpreted as an approximate estimate of the fraction exposed at the particle surface, from which the PEG coverage can be inferred.

Based on the deviation between the model intensity ratios and those observed from the C 1s fit as shown in Figure 2, the sample is closest to the oriented case when measured under cryogenic conditions. This would indicate approximately 60% coverage of the LNP surface with PEG. Although it cannot be ruled out that the additional PEG signal in the cryo-XPS results may contain a contribution from free PEG in solution, this should cause the relative proportions of C 1s signal arising from the PEG to be closer to the homogeneous model, which is not observed.

In the dry state, neither model provides results comparable to the experimental data, with the observed CC concentration beyond what would be expected from the homogeneous model. The remaining excess CC likely arises from the other lipids within the particles, which are not separable within the fit due to the lack of unique chemical species.

CONCLUSIONS

Here we have demonstrated that cryo-XPS has the ability to localise, identify and quantify the surface chemistry of two drug-delivery systems, namely polymeric nanoparticles and LNPs. To the best of our knowledge, this is the first time that cryo-XPS has been used to measure medically relevant organic nanoparticles. Significant differences in the surface carbon chemical environments were observed between the frozen hydrated samples and the room temperature, dry samples. The results for the cryo-XPS analysis are consistent with the expected structure of the system *in situ*, and which may be used to quantify features such as amount and/or completeness of a PEG coating. Cryo-XPS thus shows significant potential for providing quantitative surface chemical analysis for organic nanomedicines, which might otherwise be unsuited for analysis under vacuum. Direct quantification of oxygen content remains a limitation for this method, however, due to the significant contribution from the aqueous environment which may not be straightforward to distinguish from oxygen present in the sample. In comparison to other cryogenic techniques used for nanomedicine analysis, such as cryo-TEM and cryo-SIMS, cryo-XPS remains at an early stage of development; further work is required in order to develop the underpinning metrology, such as operating procedures, documentary standards, and reference materials.

CRediT AUTHOR STATEMENT

David Cant: Conceptualisation, Methodology, Formal analysis, Investigation, Writing – Original Draft, Project administration; **Yiwen Pei:** Resources, Writing – Review and Editing; **Andrey Shchukarev:** Investigation, Writing – Review and Editing; **Madeleine Ramstedt:** Investigation, Writing – Review and Editing; **Sara Marques:** Resources, Writing – Review and Editing; **Marcela Segundo:** Resources, Writing – Review and Editing; **Jeremie Parot:** Resources, Writing – Review and Editing; **Alicja Molska:** Resources, Writing – Review and Editing; **Sven**

Borgos: Resources, Writing – Review and Editing; **Alex Shard:** Formal analysis, Writing – Review and Editing; **Caterina Minelli:** Conceptualisation, Supervision, Funding Acquisition, Writing – Review and Editing.

Corresponding Authors

David J.H. Cant – david.cant@npl.co.uk

Caterina Minelli – caterina.minelli@npl.co.uk

SUPPLEMENTARY INFORMATION

Chemical structures for the materials used; survey spectra for both samples types in the cryo- and dry states; oxygen 1s spectra of the cryogenically prepared samples; homogeneous-equivalent atomic concentrations for both samples in cryo- and dry states; tables of intensities for the components used in the carbon 1s peak fits.

ACKNOWLEDGEMENTS

This work was funded by the National Measurement System programme of the UK Department of business, Energy and Industrial Strategy, and has received funding from the European Union's Horizon 2020 Research and Innovation Programme under grant agreement no 825828 (EXPERT). S. S. Marques and M. A. Segundo acknowledge funding from Fundação para a Ciência e a Tecnologia (FCT) and Ministério da Ciência, Tecnologia e Ensino Superior (MCTES) provided through the project EXPL/QUI-QAN/0360/2021 and in the scope of FCT Strategic Funding 2020-2023 to LAQV-REQUIMTE (UIDB/50006/2020 and UIDP/50006/2020). The authors thank Steve Spencer for his review of the manuscript.

REFERENCES

(1) Halwani, A. A. Development of Pharmaceutical Nanomedicines: From the Bench to the Market. *Pharm. 2022, Vol. 14, Page 106* **2022**, *14* (1), 106. https://doi.org/10.3390/PHARMACEUTICS14010106.

(2) Mitchell, M. J.; Billingsley, M. M.; Haley, R. M.; Wechsler, M. E.; Peppas, N. A.; Langer, R. Engineering Precision Nanoparticles for Drug Delivery. *Nat. Rev. Drug Discov. 2020 202* **2020**, *20* (2), 101–124. https://doi.org/10.1038/s41573-020-0090-8.

(3) Minelli, C.; Lowe, S. B.; Stevens, M. M. Engineering Nanocomposite Materials for Cancer Therapy. *Small* **2010**, *6* (21), 2336–2357. https://doi.org/10.1002/smll.201000523.

(4) Ferrari, M. Cancer Nanotechnology: Opportunities and Challenges. *Nat. Rev. Cancer* **2005**, *5* (3), 161–171. https://doi.org/10.1038/nrc1566.

(5) Chan, J. M.; Zhang, L.; Yuet, K. P.; Liao, G.; Rhee, J.-W.; Langer, R.; Farokhzad, O. C. PLGA-Lecithin-PEG Core-Shell Nanoparticles for Controlled Drug Delivery. *Biomaterials* **2009**, *30* (8), 1627–1634. https://doi.org/10.1016/j.biomaterials.2008.12.013.

(6) O'Neal, D. P.; Hirsch, L. R.; Halas, N. J.; Payne, J. D.; West, J. L. Photo-Thermal Tumor Ablation in Mice Using near Infrared-Absorbing Nanoparticles. *Cancer Lett.* **2004**, *209* (2), 171–176. https://doi.org/10.1016/j.canlet.2004.02.004.

(7) Tenchov, R.; Bird, R.; Curtze, A. E.; Zhou, Q. Lipid Nanoparticles from Liposomes to MRNA Vaccine Delivery, a Landscape of Research Diversity and Advancement. *ACS Nano* **2021**, *15* (11), 16982–17015. https://doi.org/10.1021/ACSNANO.1C04996/ASSET/IMAGES/MEDIUM/NN1C04996_002

6.GIF.

(8) Matsumura, Y.; Maeda, H. A New Concept for Macromolecular Therapeutics in Cancer Chemotherapy: Mechanism of Tumoritropic Accumulation of Proteins and the Antitumor Agent Smancs1. *Cancer Res.* **1986**, *46* (12_Part_1), 6387–6392.

(9) Petros, R. A.; DeSimone, J. M. Strategies in the Design of Nanoparticles for Therapeutic Applications. *Nat. Rev. Drug Discov.* **2010**, *9* (8), 615–627. https://doi.org/10.1038/nrd2591.

(10) Peer, D.; Karp, J. M.; Hong, S.; Farokhzad, O. C.; Margalit, R.; Langer, R. Nanocarriers as an Emerging Platform for Cancer Therapy. *Nat. Nanotechnol. 2007 212* **2007**, *2* (12), 751–760. https://doi.org/10.1038/nnano.2007.387.

(11) Akiyama, Y.; Mori, T.; Katayama, Y.; Niidome, T. Conversion of Rod-Shaped Gold Nanoparticles to Spherical Forms and Their Effect on Biodistribution in Tumor-Bearing Mice. *Nanoscale Res. Lett.* **2012**, *7* (1), 1–6. https://doi.org/10.1186/1556-276X-7-565/FIGURES/4.

(12) Chamundeeswari, M.; Jeslin, J.; Verma, M. L. Nanocarriers for Drug Delivery Applications. *Environ. Chem. Lett. 2018 172* **2018**, *17* (2), 849–865. https://doi.org/10.1007/S10311-018-00841-1.

(13) Shi, D.; Beasock, D.; Fessler, A.; Szebeni, J.; Ljubimova, J. Y.; Afonin, K. A.; Dobrovolskaia, M. A. To PEGylate or Not to PEGylate: Immunological Properties of Nanomedicine's Most Popular Component, Polyethylene Glycol and Its Alternatives. *Adv. Drug Deliv. Rev.* **2022**,

180, 114079. https://doi.org/10.1016/J.ADDR.2021.114079.

(14) Bertrand, N.; Grenier, P.; Mahmoudi, M.; Lima, E. M.; Appel, E. A.; Dormont, F.; Lim, J.-M.; Karnik, R.; Langer, R.; Farokhzad, O. C. Mechanistic Understanding of in Vivo Protein Corona Formation on Polymeric Nanoparticles and Impact on Pharmacokinetics. *Nat. Commun.* **2017**, *8* (1), 777. https://doi.org/10.1038/s41467-017-00600-w.

(15) Kulkarni, J. A.; Witzigmann, D.; Chen, S.; Cullis, P. R.; Van Der Meel, R. Lipid Nanoparticle Technology for Clinical Translation of SiRNA Therapeutics. *Acc. Chem. Res.* **2019**, *52* (9), 2435–2444. https://doi.org/10.1021/ACS.ACCOUNTS.9B00368/ASSET/IMAGES/MEDIUM/AR9B00368_0005.GIF.

(16) Chen, C.; Han, D.; Cai, C.; Tang, X. An Overview of Liposome Lyophilization and Its Future Potential. *J. Control. Release* **2010**, *142* (3), 299–311. https://doi.org/10.1016/J.JCONREL.2009.10.024.

(17) Zhang, J.; Brown, J.; Scurr, D. J.; Bullen, A.; MacLellan-Gibson, K.; Williams, P.; Alexander, M. R.; Hardie, K. R.; Gilmore, I. S.; Rakowska, P. D. Cryo-OrbiSIMS for 3D Molecular Imaging of a Bacterial Biofilm in Its Native State. *Anal. Chem.* **2020**, *92* (13), 9008–9015. https://doi.org/10.1021/acs.analchem.0c01125.

(18) Newell, C. L.; Vorng, J.; MacRae, J. I.; Gilmore, I. S.; Gould, A. P. Cryogenic OrbiSIMS Localizes Semi-Volatile Molecules in Biological Tissues. *Angew. Chemie Int. Ed.* **2020**, *59* (41), 18194–18200. https://doi.org/10.1002/anie.202006881.

(19) Shchukarev, A.; Ramstedt, M. Cryo-XPS: Probing Intact Interfaces in Nature and Life. *Surf. Interface Anal.* **2017**, *49* (4), 349–356. https://doi.org/10.1002/SIA.6025.

(20) Tiwari, P.; Srivastava, A. K.; Khattak, B. Q.; Verma, S.; Upadhyay, A.; Sinha, A. K.; Ganguli, T.; Lodha, G. S.; Deb, S. K. Structural Modification of Poly (Methyl Methacrylate) Due to Electron Irradiation. *Meas. J. Int. Meas. Confed.* **2014**, *51* (1), 1–8. https://doi.org/10.1016/j.measurement.2014.01.017.

(21) Delcroix, M. F.; Zuyderhoff, E. M.; Genet, M. J.; Dupont-Gillain, C. C. Optimization of Cryo-XPS Analyses for the Study of Thin Films of a Block Copolymer (PS-PEO). *Surf. Interface Anal.* **2012**, *44* (2), 175–184. https://doi.org/10.1002/SIA.3793.

(22) Ratner, B. D.; Weathersby, P. K.; Hoffman, A. S.; Kelly, M. A.; Scharpen, L. H. Radiation-Grafted Hydrogels for Biomaterial Applications as Studied by the ESCA Technique. *J. Appl. Polym. Sci.* **1978**, *22* (3), 643–664. https://doi.org/10.1002/APP.1978.070220306.

(23) Pace, H. P.; Hannestad, J. K.; Armonious, A.; Adamo, M.; Agnarsson, B.; Gunnarsson, A.; Micciulla, S.; Sjövall, P.; Gerelli, Y.; Höök, F. Structure and Composition of Native Membrane Derived Polymer-Supported Lipid Bilayers. *Anal. Chem.* **2018**, *90* (21), 13065–13072.
https://doi.org/10.1021/ACS.ANALCHEM.8B04110/SUPPL_FILE/AC8B04110_SI_001.PDF.

(24) Shchukarev, A.; Backman, E.; Watts, S.; Salentinig, S.; Urban, C. F.; Ramstedt, M. Applying Cryo-X-Ray Photoelectron Spectroscopy to Study the Surface Chemical Composition of Fungi and Viruses. *Front. Chem.* **2021**, *9*. https://doi.org/10.3389/fchem.2021.666853.

(25) Wang, Y.-C.; Engelhard, M. H.; Baer, D. R.; Castner, D. G. Quantifying the Impact of Nanoparticle Coatings and Nonuniformities on XPS Analysis: Gold/Silver Core–Shell Nanoparticles. *Anal. Chem.* **2016**, *88* (7), 3917–3925. https://doi.org/10.1021/acs.analchem.6b00100.

(26) Cant, D. J. H.; Wang, Y.-C.; Castner, D. G.; Shard, A. G. A Technique for Calculation of Shell Thicknesses for Core-Shell-Shell Nanoparticles from XPS Data. *Surf. Interface Anal.* **2016**, *48* (5), 274–282. https://doi.org/10.1002/sia.5923.

(27) Shard, A. G. A Straightforward Method for Interpreting XPS Data from Core-Shell Nanoparticles. *J. Phys. Chem. C* **2012**, *116* (31), 16806–16813. https://doi.org/10.1021/jp305267d.

(28) Belsey, N. A.; Cant, D. J. H.; Minelli, C.; Araujo, J. R.; Bock, B.; Brüner, P.; Castner, D. G.; Ceccone, G.; Counsell, J. D. P.; Dietrich et al. Versailles Project on Advanced Materials and Standards Interlaboratory Study on Measuring the Thickness and Chemistry of Nanoparticle Coatings Using XPS and LEIS. *J. Phys. Chem. C* **2016**, *120* (42), 24070–24079. https://doi.org/10.1021/acs.jpcc.6b06713.

(29) Belsey, N. A.; Shard, A. G.; Minelli, C. Analysis of Protein Coatings on Gold Nanoparticles by XPS and Liquid-Based Particle Sizing Techniques. *Biointerphases* **2015**, *10* (1), 019012. https://doi.org/10.1116/1.4913566.

(30) Spek, S.; Haeuser, M.; Schaefer, M. M.; Langer, K. Characterisation of PEGylated PLGA Nanoparticles Comparing the Nanoparticle Bulk to the Particle Surface Using UV/Vis

Spectroscopy, SEC,1H NMR Spectroscopy, and X-Ray Photoelectron Spectroscopy. *Appl. Surf. Sci.* **2015**, *347*, 378–385. https://doi.org/10.1016/j.apsusc.2015.04.071.

(31) Franzé, S.; Selmin, F.; Samaritani, E.; Minghetti, P.; Cilurzo, F. Lyophilization of Liposomal Formulations: Still Necessary, Still Challenging. *Pharmaceutics* **2018**, *10* (3), 139. https://doi.org/10.3390/pharmaceutics10030139.

(32) Anselmo, A. C.; Mitragotri, S. Nanoparticles in the Clinic: An Update Post COVID-19 Vaccines. *Bioeng. Transl. Med.* **2021**, *6* (3), e10246. https://doi.org/10.1002/BTM2.10246.

(33) Anselmo, A. C.; Mitragotri, S. Nanoparticles in the Clinic: An Update. *Bioeng. Transl. Med.* **2019**, *4* (3), e10143. https://doi.org/10.1002/BTM2.10143.

(34) Creemers, J. H. A.; Pawlitzky, I.; Grosios, K.; Gileadi, U.; Middleton, M. R.; Gerritsen, W. R.; Mehra, N.; Rivoltini, L.; Walters, I.; Figdor, C. G. et al. Assessing the Safety, Tolerability and Efficacy of PLGA-Based Immunomodulatory Nanoparticles in Patients with Advanced NY-ESO-1-Positive Cancers: A First-in-Human Phase i Open-Label Dose-Escalation Study Protocol. *BMJ Open* **2021**, *11* (11). https://doi.org/10.1136/BMJOPEN-2021-050725.

(35) Arafa, M. PLGA Nanoparticles Entrapping Ciprofloxacin to Treat E-Fecalis Infections in Endodontics https://clinicaltrials.gov/ct2/show/results/NCT05475444 (accessed Nov 23, 2022).

(36) Algadi, H. Therapeutic Efficacy of Quercetin Versus Its Encapsulated Nanoparticle on Tongue Squamous Cell Carcinoma Cell Line https://clinicaltrials.gov/ct2/show/NCT05456022 (accessed Nov 23, 2022).

(37) Calzolai, L.; Gioria, S.; Magrì, D. Nanoparticle-based vaccines in clinical trial/use for COVID-19 and licensed for other pathogens http://data.europa.eu/89h/1575f3b3-f8e6-4f6c-a296-77e8d1be4ee1 (accessed Nov 23, 2022).

(38) Chaves, L. L.; Costa Lima, S. A.; Vieira, A. C. C.; Barreiros, L.; Segundo, M. A.; Ferreira, D.; Sarmento, B.; Reis, S. Development of PLGA Nanoparticles Loaded with Clofazimine for Oral Delivery: Assessment of Formulation Variables and Intestinal Permeability. *Eur. J. Pharm. Sci.* **2018**, *112*, 28–37. https://doi.org/10.1016/J.EJPS.2017.11.004.

(39) Seah, M. P. A System for the Intensity Calibration of Electron Spectrometers. *J. Electron Spectros. Relat. Phenomena* **1995**, *71* (3), 191–204. https://doi.org/10.1016/0368-2048(94)02275-5.

(40) Seah, M. P.; Gilmore, I. S.; Spencer, S. J. Quantitative XPS: I. Analysis of X-Ray Photoelectron Intensities from Elemental Data in a Digital Photoelectron Database. *J. Electron Spectros. Relat. Phenomena* **2001**, *120* (1–3), 93–111. https://doi.org/10.1016/S0368-2048(01)00311-5.

(41) Ramstedt, M.; Shchukarev, A. Analysis of Bacterial Cell Surface Chemical Composition Using Cryogenic X-Ray Photoelectron Spectroscopy. *Methods Mol. Biol.* **2016**, *1440*, 215–223. https://doi.org/10.1007/978-1-4939-3676-2_16.

(42) Marques, S. S.; Cant, D. J. H.; Minelli, C.; Segundo, M. A. Combining Orthogonal Measurements to Unveil Diclofenac Encapsulation into Polymeric and Lipid Nanocarriers. *Anal. Chim. Acta* **2023**, *1262*, 341234. https://doi.org/10.1016/J.ACA.2023.341234.

(43) Beamson, G.; Briggs, D. High Resolution XPS of Organic Polymers: The Scienta ESCA300 Database (Beamson, G.; Briggs, D.). *J. Chem. Educ.* **1993**, *70* (1), A25. https://doi.org/10.1021/ed070pA25.5.

(44) Lewis, K. B.; Ratner, B. D. Observation of Surface Rearrangement of Polymers Using ESCA. *J. Colloid Interface Sci.* **1993**, *159* (1), 77–85. https://doi.org/10.1006/JCIS.1993.1299.

(45) Chen, L.; Hook, D. J.; Valint, P. L.; Gardella, J. A. X-Ray Photoelectron Spectroscopy Studies of Water-Induced Surface Reorganization of Amphiphilic Poly(2-Hydroxyethyl Methacrylate-g-Dimethylsiloxane) Copolymers Using Cryogenic Sample Handling Techniques. *J. Vac. Sci. Technol. A Vacuum, Surfaces, Film.* **2008**, *26* (4), 616–623. https://doi.org/10.1116/1.2943643.

(46) Chen, C.; Clarke, M. L.; Wang, J.; Chen, Z. Comparison of Surface Structures of Poly(Ethyl Methacrylate) and Poly(Ethyl Acrylate) in Different Chemical Environments. *Phys. Chem. Chem. Phys.* **2005**, *7* (11), 2357–2363. https://doi.org/10.1039/B501910A.

(47) Cruje, C.; Chithrani, D. B. Polyethylene Glycol Functionalized Nanoparticles for Improved Cancer Treatment. *Rev. Nanosci. Nanotechnol.* **2014**, *3* (1), 20–30. https://doi.org/10.1166/RNN.2014.1042.

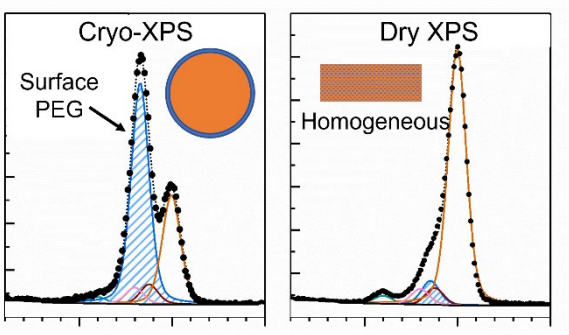

TOC Graphic